magnetochemistry

MDPI

Article

Fast Calculations for the Magnetohydrodynamic Flow and Heat Transfer of Bingham Fluids with the Hall Effect

Ye Tian [1] and Yi Liu [2,*]

[1] Key Laboratory of High-Efficiency and Clean Mechanical Manufacture of MOE, School of Mechanical Engineering, Shandong University, Jinan 250061, China
[2] School of Mathematics, Qilu Normal University, Jinan 250200, China
* Correspondence: ytwzly1996@163.com

Abstract: This study examines a mathematical model to represent the magnetohydrodynamic flow and heat transfer of Bingham fluids. The model is subject to a magnetic field's influence and incorporates the modified energy equation derived from Fourier's law. For numerical computation, we utilize the spectral collocation method in conjunction with the $L1$ algorithm to address this model. To minimize computational expenses, the sum-of-exponential technology is applied to efficiently solve the time-fractional coupled model. A specific example is provided to demonstrate the numerical method's stability and the fast method's efficiency. The results indicate that the numerical method converges with an accuracy of $O(\tau + N^{-r})$, and the fast method is highly effective in reducing computation times. Moreover, the parameters' impacts on velocity and temperature are presented and discussed graphically. It is evident that as the Hall parameter increases, the peak velocity increases and the amplitude of temperature fluctuations gradually increases, although the peak temperature decreases. The Brinkman number has a significant impact on the heat transfer rate. Meanwhile, as the Hartmann number increases, the inhibitory effect of the magnetic field on the flow is amplified.

Keywords: fastmethod; numerical calculation; fractional coupled model; Bingham fluid; magnetohydrodynamic flow and heat transfer

Academic Editor: Carlos J. Gómez García

Received: 18 February 2025
Revised: 9 March 2025
Accepted: 10 March 2025
Published: 12 March 2025

Citation: Tian, Y.; Liu, Y. Fast Calculations for the Magnetohydrodynamic Flow and Heat Transfer of Bingham Fluids with the Hall Effect. *Magnetochemistry* **2025**, *11*, 21. https://doi.org/10.3390/magnetochemistry11030021

1. Introduction

Magnetohydrodynamic (MHD) flow and heat transfer are attracting growing interest because of their broad applications across a variety of disciplines, including physics, chemistry, biology, renewable energy, and aerospace engineering. Numerous researchers have explored the dynamics of unsteady MHD flow and heat transfer, achieving notable findings [1–5]. The intricate nature of MHD flow often results in a constitutive relationship that deviates from conventional gradient laws. Therefore, traditional integer-order models are inadequate for effectively representing these "power-law phenomena". To accurately address the associated non-locality, historical effects, and path dependency, an increasing number of researchers have been incorporating fractional derivatives into MHD models. This approach provides a more comprehensive understanding of the evolution of magnetic fluids. Shahid et al. [6] performed precise calculations of velocity, temperature, and mass concentration regarding the free convection flow of a fractional MHD viscous fluid over a moving plate. Zhang et al. [7] explored the two-dimensional MHD flow and thermal transfer of fractional Oldroyd-B nanofluid between two coaxial cylinders under conditions of variable pressure. Recently, Qiao et al. [8] thoroughly examined the flow dynamics of generalized viscoelastic Maxwell fluids influenced by a periodic pressure gradient. The Bingham

fluid model, in terms of the fitting of the force–velocity relationship, effectively describes the force–velocity hysteresis and offers notable benefits. Osalusi et al. [9] investigated how viscous dissipation and Joule heating jointly influence the steady MHD and slip flow of Bingham fluids across a porous rotating disk, taking into account Hall and ion-slip currents. Similarly, Rathod et al. [10] explored the implications of heat transfer on the peristaltic MHD flow of a Bingham fluid within a channel filled with a porous medium.

Alongside the MHD flow process, heat transfer exhibits historical and dependent features that are not adequately captured by conventional Fourier law. To address this, fractional derivatives have been applied to alter Fourier's law and characterize the thermal conductivity of fluids. Povstenko et al. [11] addressed the time-fractional heat conduction equation, where fluids were subjected to specific heat flux conditions across their surfaces. Moreover, Liu et al. [12] explored the MHD issues for fractional Maxwell fluids, incorporating the fractional energy equation.

The inherent non-local characteristics of fractional derivatives, combined with the complexity of coupled models, make it quite challenging to use analytical methods for solving fractional coupled models. In recent years, various researchers have introduced numerical techniques for addressing fractional equations and coupled models [13–18]. Liu et al. [19] executed a numerical solution approach to the fractional Fitzhugh–Nagumo monodomain model, incorporating zero Dirichlet boundary conditions. Yu et al. [20] developed two effective numerical schemes to determine intermediate parameters in a fractional model, achieving second-order and fourth-order spatial accuracy. Zheng et al. [21] proposed a novel numerical methodology to address the fractional activator–inhibitor model, characterized as a coupled model. Utilizing the fast $L1$ method, Huang et al. [22] numerically addressed semi-linear time-fractional subdiffusion equations, investigating method convergence. We introduce an efficient numerical approach for solving the fractional coupled model, accurately simulating the MHD flow and heat transfer in Bingham fluids.

It is widely recognized that conventional numerical methods suffer from extended computational durations and significant computational expenses when resolving time-fractional MHD coupled models. Consequently, devising a rapid and stable method to efficiently decrease computational time is of paramount importance. Over recent years, numerous researchers and scholars have undertaken studies in this area, yielding some promising outcomes [23–29]. Alikhanov [30] constructed a new difference analog of the Caputo fractional derivative (called the $L2-1\sigma$ formula), where the convergence speed is equal to the order of approximation error. Jia et al. [31] proposed a swift finite element scheme to address the time-fractional equation of variable order. Beyond their numerical implementation, the theoretical analysis of rapid methods is also a crucial research focus. Chi et al. [32] formulated both a numerical approach and an expedited method to resolve the fractional model, which supports the rigorous convergence of the numerical scheme in conjunction with the rapid method. Among these fast methods for fractional differential operators, the research on fast methods for the $L1$ approximation formula deserves special attention. Many researchers have proposed fast calculation methods for implementing the $L1$ approximation scheme [33,34]. In this article, we consider a coupled model for the MHD flow and heat transfer process of fractional Bingham fluids. By creatively combining the $L1$ algorithm with the spectral collocation method, we propose a numerical format for solving the coupled model and establish a fast method based on the sum-of-exponential technology, effectively reducing the computation times. The numerical scheme and fast method established in this paper can effectively help us solve the fractional coupled model, improve computational efficiency, and solve large-scale computational problems in practical applications.

Two primary contributions from this paper are outlined. First, we incorporate the fractional derivative into the conduction equation, enabling the formation of a fractional coupled model to explore the MHD flow and heat transfer characteristics of Bingham fluids, influenced by a constant magnetic field. Secondly, a numerical method is developed to address the coupled model, which combines the spectral collocation method with the $L1$ algorithm. To minimize computational time and cost, a fast approach is implemented. This numerical method attains first-order convergence accuracy in the temporal domain and spectral convergence accuracy in the spatial domain, thereby significantly improving both accuracy and computational efficiency. Furthermore, the fast method substantially reduces time and expenses.

The content of the article is as follows: Section 2 addresses the physical model, introducing a fractional coupled approach. By employing the $L1$ algorithm to discretize the time-fractional derivatives in conjunction with the spectral collocation technique, Section 3 describes the construction of a fully discrete scheme to numerically solve the fractional coupled model and presents an efficient method that significantly reduces computational costs. In Section 4, we offer comprehensive examples that reinforce the effectiveness of numerical and expedited approaches. Moreover, we discuss the impact of different parameters on velocity and temperature via a numerical case study. Lastly, Section 5 outlines our conclusions.

This article investigates the MHD flow and heat transfer process of fractional Bingham fluids, which is crucial in practical applications. A Bingham fluid is a non-Newtonian fluid with yield stress characteristics, which means that the fluid will not flow until the shear stress exceeds a certain threshold. This feature makes Bingham fluids suitable for applications such as sealing, coating, and additive manufacturing that require precise flow control. It is crucial to consider the influence of magnetic fields and Hall effects on Bingham fluid flow within the framework of magnetohydrodynamics (MHD). With the influence of the Lorentz force, the magnetic field will cause changes in the distribution of velocity and temperature. At the same time, when the frequency of electron collisions is low, the Hall effect becomes significant, thereby changing the coupling mode between the magnetic field and the fluid. Therefore, in fields such as magnetic material processing, biomedicine, and metal smelting, the interaction between magnetic fields, Hall effects, and Bingham fluids can affect the optimization of key process parameters.

2. Mathematical Model

The fractional MHD Bingham fluids flow within a square cavity as illustrated in Figure 1. The length of the cavity, denoted as L_w, is significantly greater than its width, h, meaning $L_w \gg h$. The cavity is filled with Bingham fluids, and the flow is subjected to a uniform magnetic field $\mathbf{B}$. It is assumed that the boundary walls are maintained at a steady temperature T_w, and the system adheres to non-slip boundary conditions.

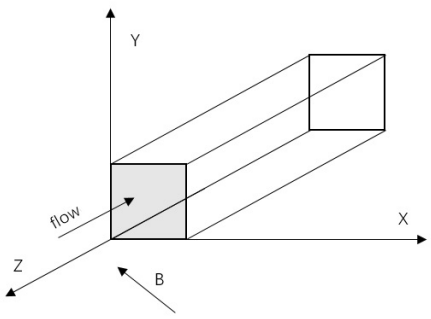

Figure 1. Schematic diagram of the physical model.

Given these assumptions, the model's velocity distribution is specified by $\mathbf{u} = (0, 0, w(x, y, t))$. The governing momentum equation is detailed in [35].

$$\nabla \cdot \mathbf{u} = 0, \tag{1}$$

$$\rho\Big(\frac{\partial \mathbf{u}}{\partial t} + (\mathbf{u} \cdot \nabla)\mathbf{u}\Big) = -\nabla p + \nabla \cdot \mathbf{S} + \mathbf{J} \times \mathbf{B}. \tag{2}$$

Here, $\mathbf{u}$ denotes the velocity vector, ρ indicates the fluid density, $\mathbf{J}$ stands for the current density, and $\mathbf{B}$ represents the constant magnetic field. The term $-\nabla p$ corresponds to the uniform pressure gradient applied to the fluid. $\mathbf{S}$ is identified as the stress tensor. Taking into account the distinctive characteristics of Bingham fluids, the constitutive equation is given by

$$S_{xz} = \mu\frac{\partial w}{\partial x}, \quad S_{yz} = \mu\frac{\partial w}{\partial y}, \tag{3}$$

where $S_{xx} = S_{xy} = S_{yy} = S_{zz} = 0$, and μ characterizes the dynamic viscosity of the Bingham fluids, usually in the form of a fraction of shear rate. It is generally observed that the viscosity of a fluid varies with its motion, thereby influencing the fluid's flow dynamics. Consequently, it is assumed herein that the viscosity of the Bingham fluid is a differentiable function. The traditional Ohm's law is modified as [36]

$$\mathbf{J} + \xi_h(\mathbf{J} \times \mathbf{B}) = \sigma(\mathbf{E} + \mathbf{u} \times \mathbf{B}), \tag{4}$$

where ξ_h denotes the Hall coefficient, $\mathbf{E}$ denotes the electric field, and σ denotes the electrical conductivity. As illustrated in Figure 1, the constant magnetic field can be written as $\mathbf{B} = (B_1, B_2, 0)$, where B_1 and B_2 are constant values. Disregarding the electric field's impact and focusing on the Hall effect, the momentum governing equation can be reformulated as

$$\frac{\partial w}{\partial t} = -\frac{1}{\rho}\frac{dp}{dz} + \frac{1}{\rho}\Big(\frac{\partial}{\partial x}(\mu\frac{\partial w}{\partial x}) + \frac{\partial}{\partial y}(\mu\frac{\partial w}{\partial y})\Big) - \frac{\sigma B_0^2}{\rho(1 + B_0^2\xi^2)}w, \tag{5}$$

where $B_0 = B_1^2 + B_2^2$.

Subsequently, we will formulate the energy equation incorporating the effects of viscous dissipation and Joule heating, as demonstrated in [2,35].

$$\rho C_p\Big(\frac{\partial T}{\partial t} + (\mathbf{u} \cdot \nabla)T\Big) = -\nabla \cdot \mathbf{q} + \mu\Big[(\frac{\partial w}{\partial x})^2 + (\frac{\partial w}{\partial y})^2\Big] + \frac{\sigma B_0^2}{1 + B_0^2\xi^2}w^2. \tag{6}$$

Here, C_p denotes the specific heat capacity. $\mathbf{q}$ stands for the heat flux, and according to the fractional Taylor formula, its derivation formula is [37]

$$\mathbf{q} + \frac{\lambda^\alpha}{\alpha!}\,{}_0D_t^\alpha\mathbf{q} = k_T\nabla T, \tag{7}$$

where k_T is the thermal conductivity. The Caputo fractional operator of order α, denoted by ${}_0D_t^\alpha$, is formally defined as [38]

$${}_0D_t^\alpha f(t) = \frac{1}{\Gamma(1-\alpha)}\int_0^t \frac{f'(s)}{(t-s)^\alpha}ds,$$

where $\Gamma(1-\alpha)$ is the value of the Gamma function at $1-\alpha$. Thus, the fractional energy equation is shown as

$$\begin{aligned}&(1+\frac{\lambda^\alpha}{\alpha!}\,{}_0D_t^\alpha)\frac{\partial T}{\partial t}\\&=\frac{k_T}{\rho C_p}\Big(\frac{\partial^2 T}{\partial x^2}+\frac{\partial^2 T}{\partial y^2}\Big)+(1+\frac{\lambda^\alpha}{\alpha!}\,{}_0D_t^\alpha)\mu\Big[(\frac{\partial w}{\partial x})^2+(\frac{\partial w}{\partial y})^2\Big]+\frac{\sigma B_0^2}{1+B_0^2\xi^2}(1+\frac{\lambda^\alpha}{\alpha!}\,{}_0D_t^\alpha)w^2.\end{aligned}\tag{8}$$

As a result of the cavity's non-slip boundary condition, the initial conditions and boundary conditions are delineated as follows:

$$w(x,y,0)=w_0(x,y),\ \ T(x,y,0)=T_w,\ \partial_t T(x,y,0)=0,\quad 0\le x,y\le h,\tag{9}$$

$$w(x,y,t)=0,\ T(x,y,t)=T_w,\quad x,y=0,\ \ x,y=h,\ \ t>0.\tag{10}$$

For convenience, we introduce the dimensionless quantities:

$$x^*=\frac{x}{h},\ \ y^*=\frac{y}{h},\ \ w^*=\frac{\mu_0 w}{h^2\frac{dp}{dz}},\ \ w_0^*=\frac{\mu_0 w_0}{h^2\frac{dp}{dz}},\ \ t^*=\frac{\mu_0 t}{\rho h^2},\ \ \lambda^*=\frac{\mu_0\lambda}{\rho h^2},\ \ \theta=\frac{T-T_w}{T_w},$$

$$Pr=\frac{C_p\mu_0}{k_T},\ \ Ha^2=\frac{\sigma B_0^2 h^2}{\mu_0},\ \ Br=\frac{h^4(\frac{dp}{dz})^2}{\mu_0^2 T_w C_p},\ \ m=\xi B_0,$$

where μ_0 represents the viscosity characteristic, Pr denotes the Prandtl number, Ha^2 corresponds to the Hartmann number, Br stands for the Brinkmann number, and m signifies the Hall number. The non-dimensional versions of Equations (5) and (8) are obtained by omitting asterisks:

$$\frac{\partial w}{\partial t}=-1+\frac{1}{\rho}\Big(\frac{\partial}{\partial x}(\mu\frac{\partial w}{\partial x})+\frac{\partial}{\partial y}(\mu\frac{\partial w}{\partial y})\Big)-\frac{Ha^2}{1+m^2}w,\tag{11}$$

$$\begin{aligned}&(1+\frac{\lambda^\alpha}{\alpha!}\,{}_0D_t^\alpha)\frac{\partial\theta}{\partial t}\\&=\frac{1}{Pr}\Big(\frac{\partial^2\theta}{\partial x^2}+\frac{\partial^2\theta}{\partial y^2}\Big)+Br(1+\frac{\lambda^\alpha}{\alpha!}\,{}_0D_t^\alpha)\mu\Big[(\frac{\partial w}{\partial x})^2+(\frac{\partial w}{\partial y})^2\Big]+\frac{Ha^2 Br}{1+m^2}(1+\frac{\lambda^\alpha}{\alpha!}\,{}_0D_t^\alpha)w^2,\end{aligned}\tag{12}$$

$$w(x,y,0)=w_0(x,y),\ \ \theta(x,y,0)=0,\ \partial_t\theta(x,y,0)=0,\quad 0\le x,y\le 1,\tag{13}$$

$$w(x,y,t)=0,\ \theta(x,y,t)=0,\quad x,y=0,\ \ x,y=1,\ \ t>0.\tag{14}$$

3. Numerical Method

In this section, we will derive the fully discrete formulation necessary to solve the coupled model Equations (11)–(14). For the discretization of time derivatives, we employ the $L1$ algorithm, while for the spatial component, we choose the spectral collocation method

$$\frac{\partial w}{\partial t}=-1+\frac{1}{\rho}\Big(\frac{\partial}{\partial x}(\mu\frac{\partial w}{\partial x})+\frac{\partial}{\partial y}(\mu\frac{\partial w}{\partial y})\Big)-\frac{Ha^2}{1+m^2}w+f_1(x,y,t),\tag{15}$$

$$\begin{aligned}&(1+\frac{\lambda^\alpha}{\alpha!}\,{}_0D_t^\alpha)\frac{\partial\theta}{\partial t}\\&=\frac{1}{Pr}\Big(\frac{\partial^2\theta}{\partial x^2}+\frac{\partial^2\theta}{\partial y^2}\Big)+Br(1+\frac{\lambda^\alpha}{\alpha!}\,{}_0D_t^\alpha)\mu\Big[(\frac{\partial w}{\partial x})^2+(\frac{\partial w}{\partial y})^2\Big]+\frac{Ha^2 Br}{1+m^2}(1+\frac{\lambda^\alpha}{\alpha!}\,{}_0D_t^\alpha)w^2\\&+f_2(x,y,t),\end{aligned}\tag{16}$$

which is subject to the initial condition

$$w(x,y,0)=w_0(x,y),\ \ \theta(x,y,0)=0,\ \partial_t\theta(x,y,0)=0,\quad (x,y)\in\Omega,\tag{17}$$

and the boundary condition

$$w(x,y,t)=0,\ \theta(x,y,t)=0,\quad (x,y)\in\partial\Omega,\ \ t>0, \tag{18}$$

where $(x,y,t)\in\Omega\times(0,\hat{T}]$, $\Omega=[0,1]\times[0,1]$.

3.1. Direct Method

In order to discretize the temporal domain, $[0,\hat{T}]$ is subdivided into equivalent segments, which leads to the formation of a time increment denoted as $\tau=\hat{T}/Q$ (Q is an integer). We establish $t_n=n\tau$ for $n=0,1,\ldots,Q$, considering $w^n(x,y)=w(x,y,t_n)$ and $\theta^n(x,y)=\theta(x,y,t_n)$. Using the $L1$ algorithm, ${}_0D_t^\alpha$ is presented [39,40].

$${}_0D_t^\alpha f(t_n)=\frac{\tau^{-\alpha}}{\Gamma(2-\alpha)}\Big[f(t_n)-\alpha_{n-1}f(t_0)-\sum_{s=1}^{n-1}(\alpha_{s-1}-\alpha_s)f(t_{n-s})\Big]+O(\tau^{2-\alpha}),$$

Here, $\alpha_s=(s+1)^{1-\alpha}-s^{1-\alpha}$ for $s=0,1,\ldots,Q$. The first-order differential operator is discretized using backward difference formulas.

$$\frac{\partial w}{\partial t}\Big|_{t=t_n}=\frac{w^n-w^{n-1}}{\tau},\quad \frac{\partial \theta}{\partial t}\Big|_{t=t_n}=\frac{\theta^n-\theta^{n-1}}{\tau}$$

By aligning two successive time steps with the terms on the right side of Equations (15) and (16), we derive

$$\frac{\partial}{\partial x}(\mu\frac{\partial w}{\partial x})\Big|=\frac{1}{2}\frac{\partial}{\partial x}(\mu^{k-1}\frac{\partial w^k}{\partial x})+\frac{1}{2}\frac{\partial}{\partial x}(\mu^{k-1}\frac{\partial w^{k-1}}{\partial x}),$$
$$\frac{\partial}{\partial y}(\mu\frac{\partial w}{\partial y})\Big|=\frac{1}{2}\frac{\partial}{\partial y}(\mu^{k-1}\frac{\partial w^k}{\partial y})+\frac{1}{2}\frac{\partial}{\partial y}(\mu^{k-1}\frac{\partial w^{k-1}}{\partial y}),$$

and

$$\Big(\frac{\partial^2\theta}{\partial x^2}+\frac{\partial^2\theta}{\partial y^2}\Big)\Big|_{t=t_n}=\frac{1}{2}\Big(\frac{\partial^2\theta^k}{\partial x^2}+\frac{\partial^2\theta^k}{\partial y^2}\Big)+\frac{1}{2}\Big(\frac{\partial^2\theta^{k-1}}{\partial x^2}+\frac{\partial^2\theta^{k-1}}{\partial y^2}\Big).$$

For convenience, we denoted $r=\frac{\lambda^\alpha\tau^{-\alpha}}{\Gamma(2-\alpha)}$, and

$$A_1=\theta^{k-1}+\sum_{s=1}^{k-1}(\alpha_{s-1}-\alpha_s)(\theta^{k-s}-\theta^{k-s-1}),\ \ A_2=\sum_{s=1}^{k-1}(\alpha_{s-1}-\alpha_s)\mu^{k-s}(\frac{\partial w^{k-s}}{\partial x})^2,$$

$$A_3=\sum_{s=1}^{k-1}(\alpha_{s-1}-\alpha_s)\mu^{k-s}(\frac{\partial w^{k-s}}{\partial y})^2,\qquad A_4=\sum_{s=1}^{k-1}(\alpha_{s-1}-\alpha_s)\mu^{k-s}(w^{k-s})^2.$$

The time semi-discrete scheme for Equations (15) and (16) when $t=t_n$ can be derived as

$$\begin{aligned}&(1+\frac{\tau Ha^2}{2(1+m^2)})w^n-\frac{\tau}{2}\frac{\partial}{\partial x}(\mu^{n-1}\frac{\partial w^n}{\partial x})-\frac{\tau}{2}\frac{\partial}{\partial y}(\mu^{n-1}\frac{\partial w^n}{\partial y})\\ =&-\tau+(1-\frac{\tau Ha^2}{2(1+m^2)})w^{n-1}+\frac{\tau}{2}\frac{\partial}{\partial x}(\mu^{n-1}\frac{\partial w^{n-1}}{\partial x})+\frac{\tau}{2}\frac{\partial}{\partial y}(\mu^{n-1}\frac{\partial w^{n-1}}{\partial y})\\ =&H_1^n(x,y),\end{aligned} \tag{19}$$

$$\begin{aligned}
&(1+r)\theta^n - \frac{\tau}{2Pr}\frac{\partial^2\theta^n}{\partial x^2} - \frac{\tau}{2Pr}\frac{\partial^2\theta^n}{\partial y^2} \\
=&\theta^{n-1} + \frac{\tau}{2Pr}\frac{\partial^2\theta^{n-1}}{\partial x^2} + \frac{\tau}{2Pr}\frac{\partial^2\theta^{n-1}}{\partial y^2} + \tau Br(1+r)\Big[\mu^n\Big((\frac{\partial w^n}{\partial x})^2 + (\frac{\partial w^n}{\partial y})^2\Big)\Big] \\
&+ \frac{\tau Ha^2 Br}{1+m^2}(1+r)(w^n)^2 + rA_1 - \tau Brr(A_2+A_3) - \frac{\tau Ha^2 Br}{1+m^2}rA_4 \\
=&H_2^n(x,y).
\end{aligned} \tag{20}$$

In the subsequent step, we employ the spectral collocation method to effectuate the discretization of the spatial dimension [41]. The set $\{(x_i,y_j)\}_{i,j=1}^N \subseteq \Omega$ should be considered, consisting of Legendre–Gauss–Lobatto nodes where $\Omega = [0,1]\times[0,1]$, with $x_1 = 0$, $x_N = 1$, $y_1 = 0$, and $y_N = 1$. The space $\mathbb{P}_N$ includes all polynomials whose degrees are less than or equal to N. Designating $\{\psi_p\}_{p=1}^N$ as the Lagrange interpolation polynomials at the nodes $\{x_p\}_{p=1}^N$, and denoting $w_{i,j}^n = w_N(x_i,y_j)$, $\theta_{i,j}^n = \theta_N(x_i,y_j)$, we can formulate $w^n(x,y)$ and $\theta^n(x,y)$ as

$$w^n(x,y) = \sum_{i=1}^N\sum_{j=1}^N \psi_i(x)w_{i,j}^n\psi_j(y), \;\; \theta^n(x,y) = \sum_{i=1}^N\sum_{j=1}^N \psi_i(x)\theta_{i,j}^n\psi_j(y).$$

Following this, the complete discrete formulation is obtained in the following manner. $w_N^n \in \mathbb{P}_N$ and $\theta_N^n \in \mathbb{P}_N$ are determined:

$$\begin{aligned}
&(1+\frac{\tau Ha^2}{2(1+m^2)})w_N^n(x_i,y_j) - \frac{\tau}{2}\frac{\partial}{\partial x}(\mu_N^{n-1}(x_i,y_j)\frac{\partial w_N^n(x_i,y_j)}{\partial x}) \\
&\quad - \frac{\tau}{2}\frac{\partial}{\partial y}(\mu_N^{n-1}(x_i,y_j)\frac{\partial w_N^n(x_i,y_j)}{\partial y}) \\
=&H_{1,N}^n(x_i,y_j),
\end{aligned} \tag{21}$$

$$(1+r)\theta_N^n(x_i,y_j) - \frac{\tau}{2Pr}\frac{\partial^2\theta_N^n(x_i,y_j)}{\partial x^2} - \frac{\tau}{2Pr}\frac{\partial^2\theta_N^n(x_i,y_j)}{\partial y^2} = H_{2,N}^n(x_i,y_j). \tag{22}$$

$$w_N^0(x_i,y_j) = w_0(x_i,y_j), \;\; \theta_N^0(x_i,y_j) = 0, \quad 1 \le i,j \le N, \tag{23}$$

$$w_N^n(x_i,y_j) = 0, \;\; \theta_N^n(x_i,y_j) = 0, \quad i,j = 1,N, \tag{24}$$

where $1 \le n \le Q$, $2 \le i,j \le N-1$, and

$$\begin{aligned}
H_{1,N}^n(x_i,y_j) =& -\tau + (1-\frac{\tau Ha^2}{2(1+m^2)})w_N^{n-1}(x_i,y_j) + \frac{\tau}{2}\frac{\partial}{\partial x}(\mu_N^{n-1}(x_i,y_j)\frac{\partial w_N^{n-1}(x_i,y_j)}{\partial x}) \\
&+ \frac{\tau}{2}\frac{\partial}{\partial y}(\mu_N^{n-1}(x_i,y_j)\frac{\partial w_N^{n-1}(x_i,y_j)}{\partial y}),
\end{aligned}$$

$$\begin{aligned}
H_{2,N}(x_i,y_j) =& \theta_N^{n-1}(x_i,y_j) + \frac{\tau}{2Pr}\frac{\partial^2\theta_N^{n-1}(x_i,y_j)}{\partial x^2} + \frac{\tau}{2Pr}\frac{\partial^2\theta_N^{n-1}(x_i,y_j)}{\partial y^2} \\
&+ \tau Br(1+r)\Big[\mu_N^n(x_i,y_j)\Big((\frac{\partial w_N^n(x_i,y_j)}{\partial x})^2 + (\frac{\partial w_N^n(x_i,y_j)}{\partial y})^2\Big)\Big] \\
&+ \frac{\tau Ha^2 Br}{1+m^2}(1+r)(w_N^n(x_i,y_j))^2 + rA_1(x_i,y_j) \\
&- \tau Brr(A_2(x_i,y_j)+A_3(x_i,y_j)) - \frac{\tau Ha^2 Br}{1+m^2}rA_4(x_i,y_j).
\end{aligned}$$

3.2. Fast Method

To lower computational expenses, we employ the sum-of-exponential (SOE) approach and introduce a swift technique that efficiently diminishes computation duration [33]. Initially, the Caputo fractional derivative is divided into two segments: the local component $C_l(t_n)$ and the history component $C_h(t_n)$. For any α, it holds that

$$\begin{aligned} D_t^{\alpha} w^n &= \frac{1}{\Gamma(1-\alpha)} \int_0^{t_n} \frac{w^{'}(s)}{(t_n - s)^{\alpha}} ds, \\ &= \frac{1}{\Gamma(1-\alpha)} \int_{t_{n-1}}^{t_n} \frac{w^{'}(s)}{(t_n - s)^{\alpha}} ds + \frac{1}{\Gamma(1-\alpha)} \int_0^{t_{n-1}} \frac{w^{'}(s)}{(t_n - s)^{\alpha}} ds, \\ &=: C_l(t_n) + C_h(t_n). \end{aligned}$$

The local component $C_l(t_n)$ can be computed by directly applying the $L1$ algorithm. The estimated expression for $C_l(t_n)$ is given as

$$C_l(t_n) \approx \frac{w^n - w^{n-1}}{\tau \Gamma(1-\alpha)} \int_{t_{n-1}}^{t_n} \frac{1}{(t_n - s)^{\alpha}} ds = \frac{w^n - w^{n-1}}{\tau \Gamma(2-\alpha)}.$$

And for the history part $C_h(t_n)$, we can obtain

$$\begin{aligned} C_h(t_n) &= \frac{1}{\Gamma(1-\alpha)} \int_0^{t_{n-1}} \frac{w^{'}(s)}{(t_n - s)^{\alpha}} ds \\ &= \frac{1}{\Gamma(1-\alpha)} \left[\frac{w^{n-1}}{\tau^{\alpha}} - \frac{w^0}{\tau^{\alpha}} - \alpha \int_0^{t_{n-1}} \frac{w(s)}{(t_n - s)^{1+\alpha}} ds \right] \\ &\approx \frac{1}{\Gamma(1-\alpha)} \left[\frac{w^{n-1}}{\tau^{\alpha}} - \frac{w^0}{\tau^{\alpha}} - \alpha \int_0^{t_{n-1}} w(s) \sum_{i=1}^{N_e} \bar{\omega}_i e^{-s_i(t_n - s)} ds \right]. \end{aligned}$$

In this setting, $\bar{\omega}_i$, s_i and N_e are positive real numbers defined in Refs. [3,33].

4. Numerical Examples

4.1. Example 1

Taking the square solution domain $\Omega = [0,1] \times [0,1]$, the precise solutions for velocity w and temperature θ are

$$w(x,y,t) = t(x^2-1)(y^2-1), \;\; \theta(x,y,t) = t^2(x-1)^2(x+1)(y-1)(y+1)^2.$$

In this condition, we take $\mu = \frac{\sqrt{2}}{(w_x + w_y)} + 1$. Initially, we delineate the values of the pertinent parameter: $Ha = 1$, $m = 1$, $\lambda = 1$, $Pr = 0.2$, and $Br = 0.1$. Furthermore, we designate $N = 16$.

Figure 2 illustrates the L^2 errors comparing the solutions for w and θ across various time steps with $\hat{T} = 1$. The numerical method for velocity and temperature described in the previous section converges at a first-order rate for any α value, indicating that the method meets accuracy requirements. Table 1 illustrates the L^2 errors and rates for both w and θ with $\alpha = 0.8$ to better convey this method's order of convergence. Then, selecting $\tau = 1/1000$ helps confirm the convergence accuracy in the spatial direction. Figure 3 presents the L^2 errors as a function of N for various α values. It is evident that the spatial L^2 error exhibits exponential decay, which indicates that our numerical approach achieves spectral accuracy in the spatial domain.

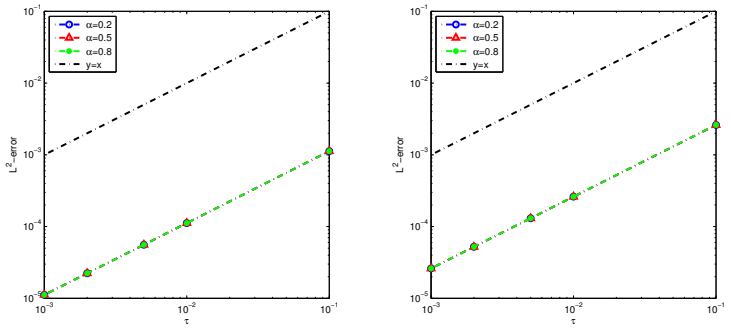

(**a**) w (**b**) θ

Figure 2. The L^2 errors of velocity w and temperature θ related to τ at $\hat{T} = 1$.

Table 1. The errors and convergence order of h at $\hat{T} = 1$ with $\tau = 1/1000$.

τ	w		θ	
	Error	**Rate**	**Error**	**Rate**
$1/10$	1.1254×10^{-3}	-	2.6136×10^{-3}	-
$1/100$	1.1181×10^{-4}	1.0028	2.6110×10^{-4}	1.0004
$1/200$	5.5873×10^{-5}	1.0008	1.3051×10^{-4}	1.0004
$1/500$	2.2352×10^{-5}	0.9986	5.2191×10^{-5}	1.0003
$1/1000$	1.1174×10^{-5}	1.0003	2.6090×10^{-5}	1.0003

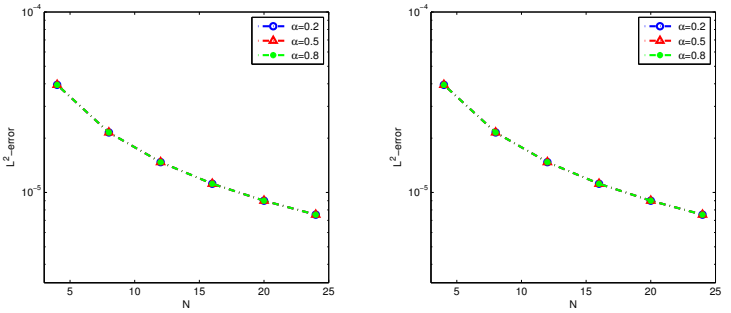

(**a**) w (**b**) θ

Figure 3. The L^2 errors of velocity w and temperature θ related to N at $\hat{T} = 1$.

To illustrate how efficient the fast method is, we use direct and fast methods to solve the time-fractional coupled model, ensuring a fast method tolerance of $N_{tol} = 10^{-5}$. Figure 4 shows the computational times for these approaches. Notably, the computation time for the fast method scales linearly with the number of steps, while the direct method's time increases at a super-linear rate. This suggests that the fast method significantly curtails the required computational time. Additionally, Figure 5 illustrates the comparison of exact solutions with the numerical solutions attained by both methods at $\tau = 1/1000$. The numerical findings for both approaches align well with the exact solutions, verifying the fast method's stability and effectiveness. Considering both accuracy and computational cost, $\tau = 1/100$ is selected for additional numerical trials.

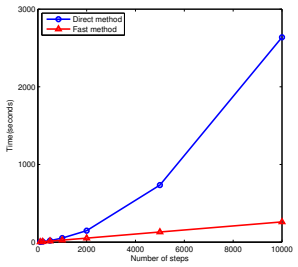

Figure 4. The computational times of the direct method and the fast method.

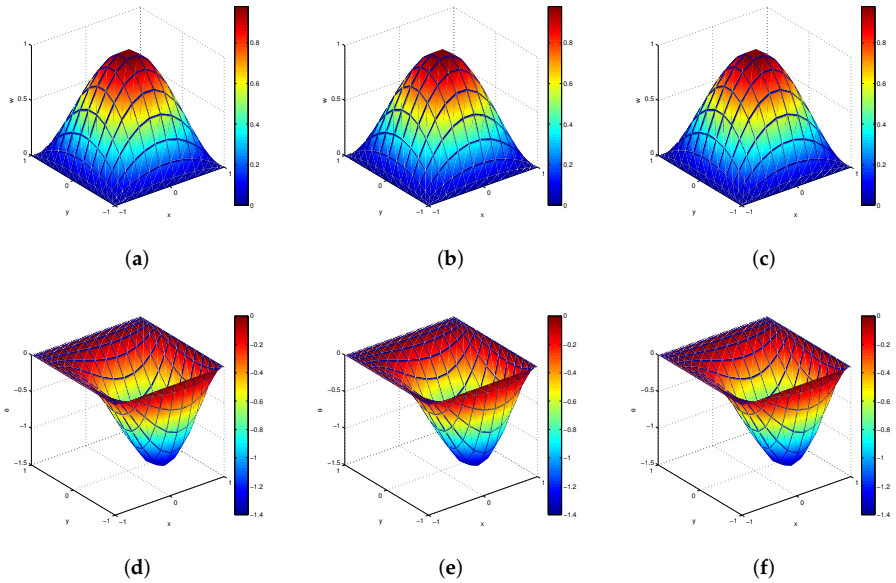

Figure 5. Exact solutions and numerical solutions obtained by the direct method and the fast method of velocity w (first row) and temperature θ (second row). (**a**) Exact solution. (**b**) Numerical solution obtained by the direct method. (**c**) Numerical solution obtained by the fast method. (**d**) Exact solution. (**e**) Numerical solution obtained by the direct method. (**f**) Numerical solution obtained by the fast method.

4.2. Example 2

Subsequently, we will set the parameters to $Ha = 1$, $m = 1$, $\lambda = 1$, $Pr = 0.2$, $Br = 0.1$, $\alpha = 0.2$ and numerically explore how different parameters influence the velocity and temperature fields. Figures 6 and 7 illustrate how the Hall effect impacts the flow and thermal transfer characteristics of a Bingham fluid confined in a square cavity, while all other parameters remain constant throughout the study. Figure 6 depicts how the velocity w changes with different Hall numbers $(m = 1,\ 3,\ 5)$. The graphs demonstrate that, for a fixed Hartmann number Ha, elevating the Hall number m results in a steady increase in maximum velocity. m modifies w by lowering the effective conductivity of the Bingham fluid $(1/(1 + m^2))$. As a result, both the Lorentz force and the Joule heat term decrease, reducing the damping effect of the fluid and improving the flow acceleration of the Bingham fluid. The vortex tends to converge towards the center, further highlighting the gradual increase in velocity. Figure 7 shows the temperature distributions with increasing Hall number m. Analyzing the graphs reveals that as m increases, the amplitude of temperature variation rises, even though the maximum temperature steadily drops. This suggests that Ha^2 influences the rate of temperature change, amplifying the fluctuations.

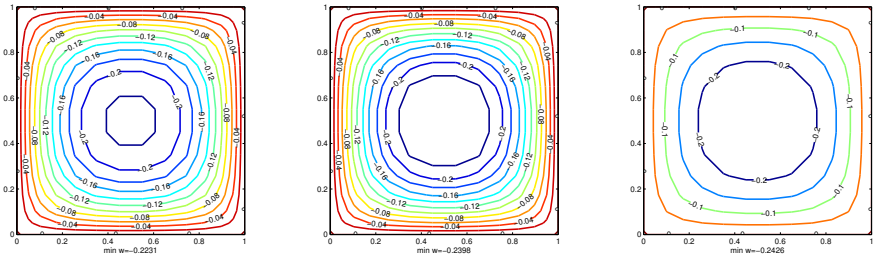

(**a**) $m = 1$ (**b**) $m = 3$ (**c**) $m = 5$

Figure 6. Isolines of velocity w under different Hall numbers.

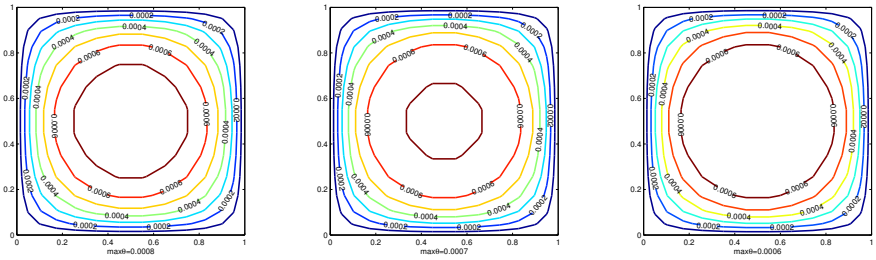

(**a**) $m = 1$ (**b**) $m = 3$ (**c**) $m = 5$

Figure 7. Isolines of temperature θ under different Hall numbers.

Figure 8 illustrates how the Brinkmann number Br impacts the temperature during the flow of a Bingham fluid within a square cavity. It is evident that Br considerably influences the heat transfer rate in the Bingham fluid. As Br rises, there is a notable increase in the fluid temperature, and the extent of this change becomes more pronounced. The presence of a non-zero Brinkmann number Br adds a nonlinear component to the fluid velocity, thereby elevating the energy dissipation and the Joule heating effect within the Bingham fluid.

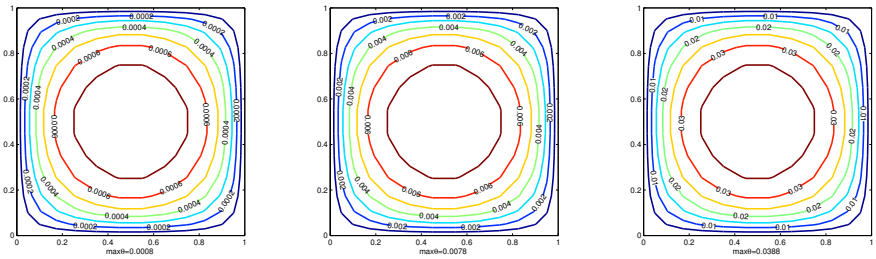

(**a**) $Br = 0.1$ (**b**) $Br = 1$ (**c**) $Br = 5$

Figure 8. Isolines of temperature θ under different Brinkmann numbers.

It is widely recognized that both conductivity and the intensity of magnetic induction significantly influence the movement of free charges in magnetic fluids. In addition to the Hall number, the Hartmann number Ha represents another critical parameter that integrates conductivity with magnetic induction intensity. Figure 9 demonstrates the velocity characteristics of Bingham fluids within a square cavity subject to various Hartmann numbers Ha in the presence of a magnetic field. The analyses indicate that, with a fixed Hall parameter m, an escalation in the Hartmann number Ha substantially reduces the flow intensity of the Bingham fluid, resulting in a pronounced decrease in peak velocity. This phenomenon can be attributed to the fact that an elevated Ha amplifies the magnetic field's inhibitory effect on the movement of magnetic fluid, thereby restricting its flow. Figure 10 illustrates the alterations in the temperature field of Bingham fluids within a square cavity at differing Hartmann numbers Ha. Evidently, as Ha increases incrementally, the peak

value of the temperature field also rises with a tendency to converge toward the center. The variation in the Hartmann number Ha influences the Joule dissipation component in the energy equation, thereby promoting heat transfer efficiency.

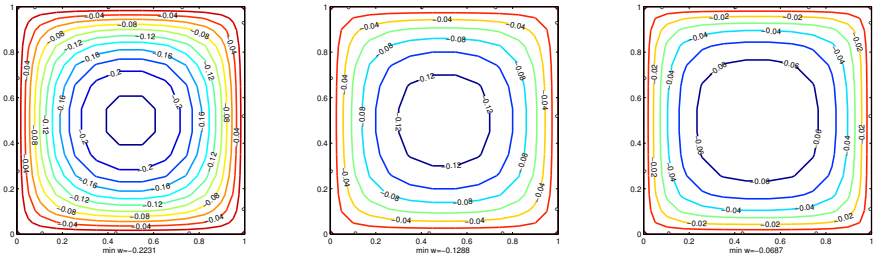

(**a**) $Ha = 1$ (**b**) $Ha = 3$ (**c**) $Ha = 5$

Figure 9. Isolines of velocity w under different Hartmann numbers.

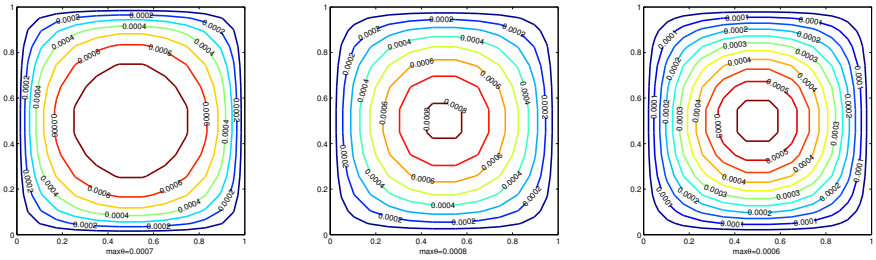

(**a**) $Ha = 1$ (**b**) $Ha = 3$ (**c**) $Ha = 5$

Figure 10. Isolines of temperature θ under different Hartmann numbers.

5. Conclusions

In this study, we present a mathematical model to clarify the MHD flow and thermal transfer of Bingham fluids under a constant magnetic field. By integrating the time-fractional operator into the constitutive equation, we formulate the time-fractional coupled model. For numerical implementation, we adopt a computational strategy using the spectral collocation method combined with the $L1$ algorithm. The numerical approach achieves first-order convergence accuracy in time and spectral convergence accuracy in space. Utilizing the sum-of-exponential (SOE) method, we devise a rapid method to solve the time-fractional coupled model, effectively minimizing computational times. We present a specific numerical example to validate the efficiency of the numerical approach. The results indicate that the numerical method converges with an accuracy of $O(\tau + N^{-r})$, aligning with theoretical predictions. The fast method is both stable and efficient in reducing computational costs. Moreover, the effects of various parameters on velocity and temperature profiles are illustrated graphically and analyzed in detail. It is clear that as m increases, the maximum velocity rises, and the amplitude of temperature fluctuations gradually increases, although the peak temperature decreases. The Brinkmann number Br substantially influences the heat transfer rate of Bingham fluids. Moreover, as the Hartmann number Ha increases, the restraining effect of the magnetic field on the magnetic fluid flow is amplified, causing a marked reduction in flow intensity and a rapid decrease in peak velocity. However, the peak temperature value tends to increase, moving toward convergence at the center. The numerical scheme introduced in this work can potentially be applied to other time-fractional partial differential models. In future investigations, we plan to develop higher-order and accelerated numerical methods to efficiently reduce computational time for solving fractional MHD coupled models.

Author Contributions: Conceptualization, Y.L.; methodology, Y.T. and Y.L.; software, Y.T. and Y.L.; writing—original draft preparation, Y.T.; writing—review and editing, Y.L.; supervision, Y.L. All authors have read and agreed to the published version of the manuscript.

Funding: This work was supported by the Natural Science Foundation of Shandong Province (ZR2024QA237).

Data Availability Statement: The data that support the findings of this study are available from the corresponding author upon reasonable request.

Conflicts of Interest: The authors declare no conflicts of interest.

References

1. Dehghan, M.; Abbaszadeh, M. Analysis of the element free Galerkin (EFG) method for solving fractional cable equation with Dirichlet boundary condition. *Appl. Numer. Math.* **2016**, *109*, 208–234. [CrossRef]
2. Wang, X.; Xu, H.; Qi, H. Transient magnetohydrodynamic flow and heat transfer of fractional Oldroyd-B fluids in a microchannel with slip boundary condition. *Phys. Fluids* **2020**, *32*, 103104. [CrossRef]
3. Liu, Y.; Zhang, H.; Jiang, X. Fast evaluation for magnetohydrodynamic flow and heat transfer of fractional Oldroyd-B fluids between parallel plates. *ZAMM-J. Appl. Math. Mech./Z. Angew. Math. Mech.* **2021**, *101*, e202100042. [CrossRef]
4. Jiang, Y.; Sun, H.; Bai, Y.; Zhang, Y. MHD flow, radiation heat and mass transfer of fractional Burgers' fluid in porous medium with chemical reaction. *Comput. Math. Appl.* **2022**, *115*, 68–79. [CrossRef]
5. Vishalakshi, A.B.; Mahesh, R.; Mahabaleshwar, U.S.; Rao, A.K.; Pérez, L.M.; Laroze, D. MHD hybrid nanofluid flow over a stretching/shrinking sheet with skin friction: Effects of radiation and mass transpiration. *Magnetochemistry* **2023**, *9*, 118. [CrossRef]
6. Shahid, N. A study of heat and mass transfer in a fractional MHD flow over an infinite oscillating plate. *SpringerPlus* **2015**, *4*, 640. [CrossRef]
7. Zhang, Y.; Jiang, J.; Bai, Y. MHD flow and heat transfer analysis of fractional Oldroyd-B nanofluid between two coaxial cylinders. *Comput. Math. Appl.* **2019**, *78*, 3408–3421. [CrossRef]
8. Qiao, Y.; Wang, X.; Xu, H.; Qi, H. Numerical analysis for viscoelastic fluid flow with distributed/variable order time fractional Maxwell constitutive models. *Appl. Math. Mech.* **2021**, *42*, 1771–1786. [CrossRef]
9. Osalusi, E.; Side, J.C.; Harris, R.E.; Johnston, B. On the effectiveness of viscous dissipation and Joule heating on steady MHD and slip flow of a Bingham fluid over a porous rotating disk in the presence of Hall and ion-slip currents. *JP J. Heat Mass Transf.* **2007**, *1*, 303–330. [CrossRef]
10. Rathod, V.P.; Laxmi, D.V. Effects of heat transfer on the peristaltic MHD flow of a Bingham fluid through a porous medium in a channel. *Int. J. Biomath.* **2014**, *7*, 1450060. [CrossRef]
11. Povstenko, Y.; Kyrylych, T. Time-Fractional Heat Conduction in a Plane with Two External Half-Infinite Line Slits under Heat Flux Loading. *Symmetry* **2019**, *11*, 689. [CrossRef]
12. Liu, Y.; Chi, X.; Xu, H.; Jiang, X. Fast method and convergence analysis for the magnetohydrodynamic flow and heat transfer of fractional Maxwell fluid. *Appl. Math. Comput.* **2022**, *430*, 127255. [CrossRef]
13. Zhang, H.; Liu, F.; Phanikumar, M.S.; Meerschaert, M.M. A novel numerical method for the time variable fractional order mobile-immobile advection-dispersion model. *Comput. Math. Appl.* **2013**, *66*, 693–701. [CrossRef]
14. Zeng, F.; Liu, F.; Li, C.; Burrage, K.; Turner, I.W.; Anh, V.V. A Crank-Nicolson ADI Spectral Method for a Two-Dimensional Riesz Space Fractional Nonlinear Reaction-Diffusion Equation. *SIAM J. Numer. Anal.* **2014**, *52*, 2599–2622. [CrossRef]
15. Ji, C.; Dai, W.; Sun, Z. Numerical Method for Solving the Time-Fractional Dual-Phase-Lagging Heat Conduction Equation with the Temperature-Jump Boundary Condition. *J. Sci. Comput.* **2018**, *75*, 1307–1336. [CrossRef]
16. Jajarmi, A.; Ghanbari, B.; Baleanu, D. A new and efficient numerical method for the fractional modeling and optimal control of diabetes and tuberculosis co-existence. *Chaos* **2019**, *29*, 093111. [CrossRef]
17. Kumar, S.; Ahmadian, A.; Kumar, R.; Kumar, D.; Singh, J.; Baleanu, D.; Salimi, M. An Efficient Numerical Method for Fractional SIR Epidemic Model of Infectious Disease by Using Bernstein Wavelets. *Mathematics* **2020**, *8*, 558. [CrossRef]
18. Yang, S.; Liu, F.; Feng, L.; Turner, I.W. Efficient numerical methods for the nonlinear two-sided space-fractional diffusion equation with variable coefficients. *Appl. Numer. Math.* **2020**, *157*, 55–68. [CrossRef]
19. Liu, F.; Turner, I.W.; Anh, V.V.; Yang, Q.; Burrage, K. A numerical method for the fractional Fitzhugh–CNagumo monodomain model. *Sci. Eng. Fac.* **2013**, *54*, C608–C629.
20. Yu, B.; Jiang, X.; Qi, H. Numerical method for the estimation of the fractional parameters in the fractional mobile/immobile advection–Cdiffusion model. *Int. J. Comput. Math.* **2018**, *95*, 1131–1150. [CrossRef]

21. Zheng, R.; Zhang, H.; Jiang, X. Legendre spectral methods based on two families of novel second-order numerical formulas for the fractional activator-inhibitor system. *Appl. Numer. Math.* **2021**, *162*, 235–248. [CrossRef]
22. Huang, Y.; Zeng, F.; Guo, L. Error estimate of the fast L1 method for time-fractional subdiffusion equations. *Appl. Math. Lett.* **2022**, *133*, 108288. [CrossRef]
23. Farquhar, M.E.; Moroney, T.J.; Yang, Q.; Turner, I.W. GPU accelerated algorithms for computing matrix function vector products with applications to exponential integrators and fractional diffusion. *SIAM J. Sci. Comput.* **2016**, *38*, C127–C149. [CrossRef]
24. Krishnarjuna, B.; Chandra, K.; Atreya, H.S. Accelerating NMR-Based Structural Studies of Proteins by Combining Amino Acid Selective Unlabeling and Fast NMR Methods. *Magnetochemistry* **2017**, *4*, 2. [CrossRef]
25. Jia, J.; Zheng, X.; Wang, H. A fast method for variable-order space-fractional diffusion equations. *Numer. Algorithms* **2019**, *85*, 1519–1540. [CrossRef]
26. Fang, Z.; Sun, H.; Wang, H. A fast method for variable-order Caputo fractional derivative with applications to time-fractional diffusion equations. *Comput. Math. Appl.* **2020**, *80*, 1443–1458. [CrossRef]
27. Cao, J.; Xiao, A.; Bu, W. Finite Difference/Finite Element Method for Tempered Time Fractional Advection–Dispersion Equation with Fast Evaluation of Caputo Derivative. *J. Sci. Comput.* **2020**, *83*, 1–29. [CrossRef]
28. Wang, P. Fast exponential time differencing/spectral-Galerkin method for the nonlinear fractional Ginzburg-Landau equation with fractional Laplacian in unbounded domain. *Appl. Math. Lett.* **2021**, *112*, 106710. [CrossRef]
29. Zhu, H.; Xu, C. A Fast High Order Method for the Time-Fractional Diffusion Equation. *SIAM J. Numer. Anal.* **2019**, *57*, 2829–2849. [CrossRef]
30. Alikhanov, A.A. A new difference scheme for the time fractional diffusion equation. *J. Comput. Phys.* **2015**, *280*, 424–438. [CrossRef]
31. Jia, J.; Wang, H.; Zheng, X. Numerical Analysis of a Fast Finite Element Method for a Hidden-Memory Variable-Order Time-Fractional Diffusion Equation. *J. Sci. Comput.* **2022**, *91*, 54. [CrossRef]
32. Chi, X.; Zhang, H.; Jiang, X. The fast method and convergence analysis of the fractional magnetohydrodynamic coupled flow and heat transfer model for the generalized second-grade fluid. *Sci. China Math.* **2023**, *67*, 919–950. [CrossRef]
33. Jiang, S.; Zhang, J.; Zhang, Q.; Zhang, Z. Fast evaluation of the Caputo fractional derivative and its applications to fractional diffusion equations. *Commun. Comput. Phys.* **2017**, *21*, 650–678. [CrossRef]
34. Xiao, J.; Chen, Y.; Zeng, F.; Zhang, Z. L1 Schemes for time-fractional differential equations: A brief survey and new development. *Res. Sq.* **2024**, *posted*.
35. Zhao, J.; Zheng, L.; Zhang, X.; Liu, F. Convection heat and mass transfer of fractional MHD Maxwell fluid in a porous medium with Soret and Dufour effects. *Int. J. Heat Mass Transf.* **2016**, *103*, 203–210. [CrossRef]
36. Cowling, T. *Magnetohydrodynaics*; Interscience: New York, NY, USA, 1957.
37. Liu, Y.; Guo, B. Coupling model for unsteady MHD flow of generalized Maxwell fluid with radiation thermal transform. *Appl. Math. Mech.* **2016**, *37*, 137–150. [CrossRef]
38. Podlubny, I. *Fractional Differential Equations*; Academic Press: New York, NY, USA, 1999.
39. Sun, Z.; Wu, X. A fully discrete difference scheme for a diffusion-wave system. *Appl. Numer. Math.* **2006**, *56*, 193–209. [CrossRef]
40. Liu, L.; Yang, S.; Feng, L.; Xu, Q.; Zheng, L.; Liu, F. Memory dependent anomalous diffusion in comb structure under distributed order time fractional dual-phase-lag model. *Int. J. Biomath.* **2021**, *14*, 2150048. [CrossRef]
41. Shen, J.; Tang, T.; Wang, L. *Spectral Methods: Algorithms, Analysis and Applications*; Springer: Berlin/Heidelberg, Germany, 2011.